Chinese Journal of
POLYMER SCIENCE

RESEARCH ARTICLE

https://doi.org/10.1007/s10118-024-3143-3
Chinese J. Polym. Sci. **2024**, *42*, 1227–1242

Structural Evolution of Ultra-High Molecular Weight Polyethylene Low-Entangled Films with Reserved Shish Crystals During Hot Stretching

Jia-Wei Gao, Li Chen, Ye-Shun Zhong, Chao-Wei Xing, Yi-Guo Li, and Zong-Bao Wang*

School of Materials Science and Chemical Engineering, Ningbo University, Ningbo 315211, China

Electronic Supplementary Information

Abstract Shish crystals are crucial to achieving high performance low-dimensional ultra-high molecular weight polyethylene (UHMWPE) products. Typically, high stretch and shear flow fields are necessary for the formation of shish crystals. In this study, UHMWPE gel films with reserved shish crystals were prepared by gel molding, the structural evolution and properties of UHMWPE films stretched at temperatures of 100, 110, 120 and 130 °C were investigated by *in situ* small-angle X-ray scattering (SAXS)/ultra-small-angle X-ray scattering (USAXS)/wide-angle X-ray diffraction (WAXD) measurements as well as scanning electron microscopy (SEM) and differential scanning calorimetry (DSC) measurements. Our findings showed that the reserved shish crystals can facilitate the formation and structural evolution of shish-kebab crystals during the hot stretching. Additionally, the reserved shish crystals promote the structural evolution of UHMWPE films to a greater extent when stretched at 120 and 130 °C, compared to 100 and 110 °C, resulting in higher crystallinity, orientation, thermal properties, breaking strength and Young's modulus. Compared to UHMWPE high-entangled films with reserved shish crystals prepared by compression molding, UHMWPE low-entangled films with reserved shish crystals prepared by gel molding are more effective in inducing the formation and evolution of shish-kebab crystals during the hot stretching, resulting in increased breaking strength and Young's modulus.

Keywords UHMWPE low-entangled films; Reserved shish crystals; Structural evolution; Hot stretching

Citation: Gao, J. W.; Chen, L.; Zhong, Y. S.; Xing, C. W.; Li, Y. G.; Wang, Z. B. Structural evolution of ultra-high molecular weight polyethylene low-entangled films with reserved shish crystals during hot stretching. *Chinese J. Polym. Sci.* **2024**, *42*, 1227–1242.

INTRODUCTION

Ultra-high molecular weight polyethylene (UHMWPE) products are often processed under the coupling of multiple flow fields, the properties of UHMWPE products are closely related to the chain orientation and crystal formation in the flow field. When the molecular chains are highly oriented in the flow fields, it can lead to the formation of shish-kebab crystals, which may even transform into shish crystals, resulting in increased mechanical properties of the UHMWPE products.[1–5] UHMWPE low-dimensional products, such as UHMWPE fibers, are composed of highly oriented shish crystals, resulting in excellent tensile strength and tensile modulus, therefore, it is widely used in protective equipment, aerospace and marine engineering.[6–13] As a result, the formation and evolution of shish-kebab crystals in low-dimensional UHMWPE products is crucial to the improvement of their mechanical properties.

In the recent years, researchers have conducted extensive research on the structural evolution of low-dimensional UHMWPE products, especially the formation and evolution of shish-kebab crystals. Keum *et al*.[14] found the high melting temperature of shish indicates that the shish stability is mainly controlled by the thermodynamics of stretched chains under the planar constrained conditions. Xu *et al*.[15] found the UHMWPE interlocking state significantly enhances the interfacial adhesion between separate shish-kebab superstructure and also provides a tendency to homogenize properties of the samples in all directions. Zhang *et al*.[16] found the UHMWPE long chains enable the appearance of lamellae orientation and shish-kebab crystalline morphology in the injection molded process, which are responsible for the mechanical reinforcement. Kakiage *et al*.[17] investigated UHMWPE fibers prepared by melting spinning through melt stretching at a temperature of 145 °C, they found that the higher strain rates facilitated the extension of molecular chains and the formation of shish crystals, resulting in increased tensile strength of the fibers. Albert *et al*.[18] observed the elongation of molecular chains and the formation of shish crystals, drawing the UHMWPE gel fibers at room temperature to a draw ratio of 6 results in the fracturing and tilting of the lamellae, as well as the formation of a large number of shish-kebab structures. Jen *et al*.[19] investigated the effect of stretch ratio on the mor-

* Corresponding author, E-mail: wangzongbao@nbu.edu.cn
Received February 27, 2024; Accepted April 12, 2024; Published online May 10, 2024

© Chinese Chemical Society
Institute of Chemistry, Chinese Academy of Sciences

phology and crystal phase transition of gel UHMWPE fibers by wide-angle X-ray diffraction (WAXD), which showed that the kebab crystals of the UHMWPE fiber were gradually transformed into the highly oriented shish crystals when the stretch ratio increased from 1 to 20. Moreover, the kebab crystals were almost unobservable on the surface of the UHMWPE fibers, and only shish crystals could be observed when the stretch ratio increased from 20 to 40. Our group[20] investigated the evolution of kebab crystals and the formation of shish crystals during a two-step hot stretching process (at the temperatures of 120 and 130 °C) of UHMWPE fibers obtained from industrial production lines by WAXD and small-angle X-ray scattering (SAXS). The results showed that kebab structure was reduced with the increase of stretching ratio during the first step, while the increase of temperature during the second step could accelerate the evolution from kebab to shish crystal. We[21] also investigated the influence of hot stretching temperature and stretching ratio on the formation of shish crystals in UHMWPE fibers by *in situ* SAXS, the results showed that stretching at 124–130 °C resulted in the formation of shish crystals, while stretching at 140 °C, the formation of shish crystals required higher stretching ratios. And the lower stretching ratios mainly resulted in the formation of kebab crystals, while the higher stretching ratios resulted in the evolution from kebab crystals to shish crystals at all stretching temperatures. Building upon this foundation, our group[22,23] further investigated the transition from shish-kebab crystals to shish crystals during hot stretching of UHMWPE fibers prepared by low and high concentration solutions, for fibers with low concentration, the lamellae transformed into shish crystals through the stress-induced fragmentation and recrystallization at 90, 100 and 110 °C, and stress-induced melting and recrystallization at 120 °C with the increase of hot-stretching strain, and the shish-kebab crystals could smoothly transform to shish crystals through the hot stretching process. For fibers with high concentration, the shish-kebab crystals in UHMWPE fibers could transform continuously into the micro-fibril structure composed mainly of shish crystals during the hot stretching.

The formation and evolution of shish-kebab crystals are crucial to the structural evolution and properties of UHMWPE products. In fact, the formation of shish-kebab crystals occurs during the synthesis of UHMWPE resins. Several studies have consistently reported the presence of extended chain crystals in the nascent UHMWPE resin within the Ziegler-Natta catalytic system,[24–26] which is similar to the catalytic system used in the manuscript. Yu *et al*.[27,28] found that the active sites and polymer chains of the initial UHMWPE resins synthesized from POSS-modified heterogeneous Ziegler-Natta catalysts were separated. The molecular chains showed weak entanglement and high linearity, which could induce the formation of shish-kebab crystals. Dermeneva *et al*.[29] found that the resin consisted mainly of fibrous and lamellar crystals. Chanzy *et al*.[30,31] noted the different melting points of fibrous and lamellar crystals. Ingram *et al*.[32,33] also found fibrous crystals in nascent UHMWPE resin prepared by the Ziegler-Natta catalytic system. Our group conducted dissolution and crystallization experiments on UHMWPE resins in paraffin oil. The experiments found a large number of shish-kebab crystals, which further proved the existence of extended chain crystals in the nascent resins.

Studying how to better use shish crystals in the processing of UHMWPE to improve the properties of UHMWPE products have become a research topic for many scientists. Hiroki *et al*.[34] found that the shish crystals which formed in weak flow fields can serve as nucleating agents to increase the mechanical properties of final products in melt injection molding and blow molding. Pircheraghi *et al*.[35] discovered the fiber-like crystals on the fracture surfaces of UHMWPE sheets by sintering at different temperatures, which induced the formation of kebab crystals. Lame *et al*.[36] found that the UHMWPE sheets exhibited numerous fibrous crystals in the SEM results after melt processing of UHMWPE by high speed and multiple hot pressing, which provided products with high modulus and high ductility. Our group[37,38] found that the addition of fibrous chitin nanocrystals to the UHMWPE fibers could accelerate the stress-induced fragmentation and recrystallization at 90, 100 and 110 °C, and stress-induced melting and recrystallization at 120 °C, resulting in the formation of more fibrous crystals. It is evident that both fiber-like crystals formed during processing and introduced fiber-like nucleating agents significantly influence the structural evolution and properties of UHMWPE products. On this basis, our group[39,40] reserved the original shish crystals in the UHMWPE resins and prepared the UHMWPE films with reserved shish crystals by compression molding, the results showed that reserved shish crystals could directly induce the formation of more and longer shish crystals, resulting in a significant improvement in the mechanical properties of the final film.

Reserved shish crystals during compression molding can accelerate the structural evolution and improve the properties of UHMWPE films, but the high-entangled molecular chains and film uniformity problems during compression molding significantly affect the crystal structure and morphology of UHMWPE films, which ultimately limits the further improvement of the mechanical properties of the UHMWPE films.[41–45] Until now, the main process of low-dimensional UHMWPE products is gel molding, which allows significant disentanglement of the molecular chains in the plasticizing environment of the solvent, and keep the disentangled molecular chains in the gel products. Subsequently, low-entangled UHMWPE products were formed by solvent extraction. The gel molding process facilitates the disentanglement of molecular chains and the formation and evolution of shish-kebab crystals. This provides the basis for preparing UHMWPE fibers with improved properties.[46–50] Therefore, we prepared the UHMWPE low-entangled films with reserved shish crystals by gel molding, using the dissolution temperature difference between shish crystals and lamellae. The shish crystals reserved by the dissolution process can directly contribute to the formation and evolution of shish-kebab crystals during hot stretching, which avoids the effect of high-entangled molecular chains during the structural evolution. Notably, the structural evolution of UHMWPE extracted films with reserved shish crystals in a low-entangled system during hot stretching remains unexplored.

This study investigated the mechanisms of the structural evolution during hot stretching of UHMWPE low-entangled films. UHMWPE low-entangled films with reserved shish crys-

tals and without were prepared by gel molding at the temperature of 133 and 200 °C, respectively. The structural evolution of UHMWPE low-entangled films subjected to uniaxial stretching during hot stretching was investigated by *in situ* SAXS/WAXD/ultra-small-angle X-ray scattering (USAXS) and scanning electron microscopy (SEM) and differential scanning calorimetry (DSC).

EXPERIMENTAL

Materials and Sample Preparation

The UHMWPE resin, with a viscosity-average molecular weight ($\bar{M}_v$) of 1.9×10^6 g/mol, was provided by the Shanghai Institute of Organic Chemistry, Chinese Academy of Sciences. The paraffin oil A360B was purchased from Total Energies with a flash point of 250 °C. A mixture of UHMWPE resins and paraffin oil in a 1:9 (*W*:*W*) proportion was dissolved using a twin-screw extruder at temperatures of 133 and 200 °C before being extruded through a flat mouth die of dimensions 30 mm × 0.5 mm. The extruded material was then cooled *via* mirrored rolls, to obtain the initial UHMWPE gel films. Following this, a 4-h extraction with *n*-hexane solvent was performed, the resulting UHMWPE low-entangled films were vacuum-dried for 6 h at 70 °C. During these processes, the films were carefully maintained in a taut state to prevent shrinkage.

In situ Small-angle X-ray Scattering (SAXS)/ Wide-angle X-ray Diffraction (WAXD) and Ultra-small-angle X-ray Scattering (USAXS) Measurements

In situ SAXS and WAXD measurements were performed at the BL16B1 beamline of the Shanghai Synchrotron Radiation Facility (SSRF), with X-ray wavelength set at 0.124 nm, and an exposure time of 4 s was employed. Prior to testing, blank samples were tested to obtain the background diffraction patterns for both SAXS and WAXD. The patterns for 2D-SAXS and 2D-WAXD were captured using Pilatus 900K and Pilatus 2M detectors with a resolution of 172 μm × 172 μm. The sample-to-detector distances for SAXS and WAXD modes were calibrated to 242 and 1676 mm, respectively, using silver behenate (AgBe) and cerium dioxide (CeO_2) for standard samples. We used a Linkam, MFS350 stretching device to perform uniaxial stretching at temperatures of 100, 110, 120 and 130 °C with a stretching speed of 5mm·min^{-1}. During stretching, we simultaneously recorded stress-strain curves and X-ray data. The length of the film between the stretching fixtures was 15 mm. All X-ray signals were normalized to the beam fluctuations. The WAXD and SAXS data were analyzed using FIT2D software.[51]

In situ ultra-small-angle X-ray scattering (USAXS) measurement was conducted at the BL10U1 beamline station of the SSRF. The 2D-USAXS patterns were recorded using Dectris Eiger 4M detector with a pixel resolution of 75 μm × 75 μm and an exposure time of 4 s. The distance between the sample and the detector for USAXS was calibrated using a bovine tendon standard sample, resulting in a distance of 27600 mm. The stretching parameters were consistent with those of the *in situ* SAXS/WAXD measurements. The *in situ* USAXS data were synchronously collected during the stretching process of the samples.

Scanning Electron Microscopy (SEM)

The morphology characterization of UHMWPE films under different stretching temperatures and strains was performed using SEM (SU70) at 5 kV. To prepare the SEM samples, UHMWPE film samples were heated to 105–115 °C in an *n*-octane solvent to etch the surfaces and remove the amorphous component for a clearer visibility of the film's crystal structure on the surface. The samples were then rinsed three times with anhydrous ethanol and dried. Finally, after the samples were prepared, a gold sputter coating was applied to the surface for imaging.

Differential Scanning Calorimetry (DSC)

Samples weighing 5–8 mg were held in a standard aluminum crucible by a dry nitrogen gas stream, and the thermal properties of UHMWPE films were recorded using NETZSCH Polyma DSC21400A. Prior to the actual measurements, a blank sample test was performed to eliminate any signal interference except that of the samples. The samples were heated and scanned from 25 °C to 200 °C at a ramp rate of 10 °C/min. The enthalpy of melting for 100% crystalline polyethylene is 293 J/g.[52]

Viscosity

The viscosity characterization of UHMWPE low-entangled films was performed using the rheometer (Haake Mars60). Rheological experiments were conducted on UHMWPE films (dimensions of 20 mm in diameter and 0.3 mm in thickness) using fixed strain and frequency time scans. The rheological testing process proceeds as follows: employing a parallel plate test system, the modulus test is selected with a constant strain of 0.025%, a temperature of 180 °C, a frequency of 1 Hz, and a test duration of 30 min.[47]

Breaking Strength and Young's Modulus

The UHMWPE low-entangled films with reserved shish crystals and those without were first stretched to the strain of 500%, 350%, 300% and 300% with tensile equipment (Linkam TST350) at a speed of 5 mm·min^{-1} at 100, 110, 120 and 130 °C, and then cooled to room temperature naturally. The same strains were chosen for both films with and without reserved shish crystals at the same stretching temperatures. After cooling the samples, we used the Linkam TST350 to test the breaking strength and Young's modulus of the necking section at a speed of 10 mm·min^{-1}.

SAXS/USAXS/WAXD Data Analysis

Fig. 1(a) displays the SAXS pattern of the UHMWPE film and the stretching direction, where q_1 was vertical to the stretching direction and q_2 was parallel to the stretching direction. Due to the principle of reciprocal space, the scattering signal along the q_1 direction represents the scattering signal of the crystal along the stretching direction, while the scattering signal along q_2 represents the scattering signal of the crystal vertical to the stretching direction.[14,53–56] Referring the calculation of the relative scattering intensity of shish and kebab crystals, the corresponding scattering signals of crystals along the stretching direction and vertical to the stretching direction were integrated as shown in Fig. 1(b) and Fig. 1(c), respectively. The calculation formula is as follows:

$$I_{q1} = \int_{0.03}^{0.3}\int_{-160^\circ}^{160^\circ} I(q,\phi)\,\mathrm{d}q\mathrm{d}\phi \quad (1)$$

$$I_{q2} = \int_{0.05}^{0.5}\int_{160^\circ}^{20^\circ} I(q,\phi)\,\mathrm{d}q\mathrm{d}\phi \quad (2)$$

The average shish length (L_{shish}) and the distribution of

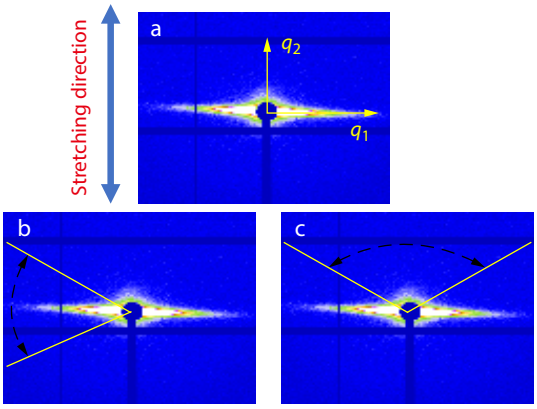

Fig. 1 (a) The SAXS patterns of UHMWPE films; (b) The scattering intensity of crystals in the stretching direction; (c) The scattering intensity of crystals in the vertical stretching direction.

shish crystals (B_ϕ) was calculated using the Ruland's streak method by analyzing the streak along the equator line direction in the USAXS patterns.[57–59] When the scattering intensity distribution fit the Lorentz functions, the equation is expressed as follows:

$$B_{obs} = \frac{1}{\langle L_{shish} \rangle s} + B_\phi \tag{3}$$

When the scattering intensity distribution fit the Gaussian functions; then, the equation becomes:

$${B_{obs}}^2 = \left(\frac{1}{\langle L_{shish} \rangle s}\right)^2 + {B_\phi}^2 \tag{4}$$

where s is the scattering vector, $s = 2\sin\theta/\lambda$.

The intensity distribution curve concerning 2θ is obtained by one-dimensional integration of the 2D-WAXD pattern. Peaking analysis is subsequently applied to the curve to calculate the proportions of the amorphous and crystalline regions, then calculates the crystallinity. The formula of calculation is as follows, where A_c and A_a represent the areas under the crystalline and amorphous peaks of the $I(2\theta)$~2θ curve.

$$X_c = \frac{A_c}{A_c + A_a} \tag{5}$$

The lateral size of the crystals was determined using the Scherrer equation. Where K is the shape factor, generally set to 0.89 in polymer science, λ is the wavelength, θ is the Bragg diffraction angle, and β is the half-peak width at maximum intensity.[60]

$$L_{hkl} = \frac{K\lambda}{\beta\cos\theta} \tag{6}$$

The crystal orientation of UHMWPE films was determined using the Herman's method. In this study, the stretching direction of the UHMWPE film was taken as the reference direction. Assuming the crystal plane as hkl, the orientation parameter can be expressed as follows:

$$< \cos^2\phi >_{hkl} = \frac{\int_0^{\pi/2} I(\phi)\cos^2\phi\sin\phi d\phi}{\int_0^{\pi/2} I(\phi)\sin\phi d\phi} \tag{7}$$

where, ϕ is the azimuth angle, and $I(\phi)$ is the scattering intensity along the azimuth angle. The orientation f can be defined as follows:

$$f = \frac{3< \cos^2\phi >_{hkl} - 1}{2} \tag{8}$$

When f=–0.5 and 1, it represents that the normal of the reflection plane is parallel or vertical to the reference direction, respectively; f=0 when the orientation is random.

RESULTS AND DISCUSSION

UHMWPE Low-entangled Films with Reserved Shish Crystals

The sample information for the UHMWPE films stretched at a rate of 5 mm·min^{-1} at temperatures of 100, 110, 120 and 130 °C is shown in Table 1. UPE-dt133 represents the UHMWPE low-entangled film with reserved shish crystals, UPE-dt200 represents the UHMWPE film without reserved shish crystals.

To characterize the degree of entangled molecular chains of the UHMWPE gel films, viscosity measurements were performed using shear rheology measurements. The viscosity values of UPE-dt200 was 2.2×10^4 Pa·s, while UPE-dt133 had a viscosity of 1.2×10^4 Pa·s, both significantly lower than the viscosity of UHMWPE compression molding samples (which had a viscosity of 1.0×10^7 Pa·s).[61] Hsien *et al.*[62] investigated UHMWPE gels with different concentrations, they found that the viscosity of the 7% UHMWPE gel was 2.5×10^4 Pa·s, while at lower concentrations (2%–6%), the viscosity was 1×10^4 Pa·s. The viscosity of UPE-dt200 and UPE-dt133 was lower than the viscosity of UHMWPE gel with a 7% concentration reported by Hsien *et al*. This suggests that the UHMWPE films prepared in this study belong to the low-entangled system. The degree of entangled molecular chains of UPE-dt133 was lower than that of UPE-dt200, this further suggests that reserved shish crystals significantly facilitate the disentanglement of molecular chains of UHMWPE gel films. The viscosity of the UHMWPE films with reserved shish crystals prepared in this study is also lower than that of the UHMWPE film with reserved shish crystals previously prepared by our group by compression molding (3.1×10^4 Pa·s). This also suggests that the UHMWPE films with reserved shish crystals prepared by gel molding in this study belong to the low-entangled system.

Fig. 2 presents the SEM morphology of UPE-dt200 and UPE-dt133. It can be observed that UPE-dt200 is composed of randomly distributed lamellae, UPE-dt133 is composed of not only randomly distributed lamellae but also multiple shish crystals, indicating that the shish crystal in the resin have been successfully reserved. Comparing the morphology of

Table 1 Dissolution and stretching temperature of UHMWPE gel films.

Dissolution temperature (°C)	Stretching temperature (°C)	Abbreviation
133	–	UPE-dt133
	100	UPE-dt133st100
	110	UPE-dt133st110
	120	UPE-dt133st120
	130	UPE-dt133st130
200	–	UPE-dt200
	100	UPE-dt200st100
	110	UPE-dt200st110
	120	UPE-dt200st120
	130	UPE-dt200st130

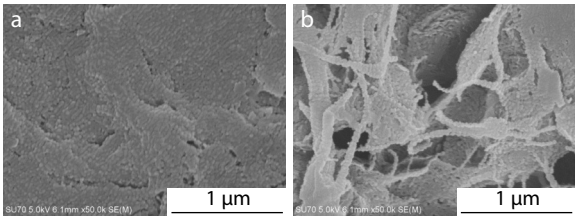

Fig. 2 SEM morphology of (a) UPE-dt200 and (b) UPE-dt133.

UHMWPE films with reserved shish crystals prepared by compression molding[39] to the UHMWPE low-entangled films with reserved shish crystals by gel molding in this study, the UHMWPE low-entangled films with reserved shish crystals by gel molding show more uniform shish crystal distribution. This difference in morphology resulting from the processing method because the plasticizer in the gel molding process, which further facilitates the disentanglement of molecular chains and improves the distribution of the reserved shish crystals.

DSC results can also confirm the successful reservation of shish crystals in UPE-dt133. As shown in Fig. 3, the melting point of UPE-dt200 reaches 138.9 °C due to the randomly distributed lamellae observed in the SEM. UPE-dt133 has two high temperature melting points at 140.1 and 142.7 °C. The high-temperature melting point of 142.7 °C corresponds to the reserved shish crystals during the gel molding, while the melting point of 140.1 °C corresponds to the lamellae that grew around the reserved shish crystals.[23] The crystallinity values of UPE-dt200 and UPE-dt133 are 68.1% and 69.6%, respectively, these values were obtained by calculating the areas under the melting points. This indicates that the lower dissolution temperature during gel molding of UPE-dt133 resulted in partial reservation of shish crystals, whereas shish crystals in UPE-dt200 were completely dissolved during gel molding. This difference also confirms the successful reservation of shish crystals in UPE-dt133. The UHMWPE low-entangled films with reserved shish crystals prepared by gel molding have two melting points at 140.1 and 142.7 °C, which are higher than the UHMWPE high-entangled films with reserved shish crystals prepared by compression molding (133.2 and 139.8 °C).[40] Compared to the UHMWPE high-entangled film with reserved shish crystals, the UHMWPE low-entangled film with reserved shish crystals prepared by gel-molding exhibits a higher melting point. This suggests that the reserved shish crystals can enhance the formation of a more perfect crystal structure in the UHMWPE low-entangled system. Additionally, since the degree of entanglement of UPE-dt200 and UPE-dt133 samples was much lower than the viscosity of UHMWPE samples prepared by compression molding as we mentioned before, and we prevent the effect of re-entanglement during the hot stretching by choosing stretching temperatures lower than the melting point of the UHMWPE samples, therefore, we did not discuss the minor effects of the entanglement state on the structural evolution and final mechanical performance of the UPE-dt200 and UPE-dt133 samples during hot stretching.

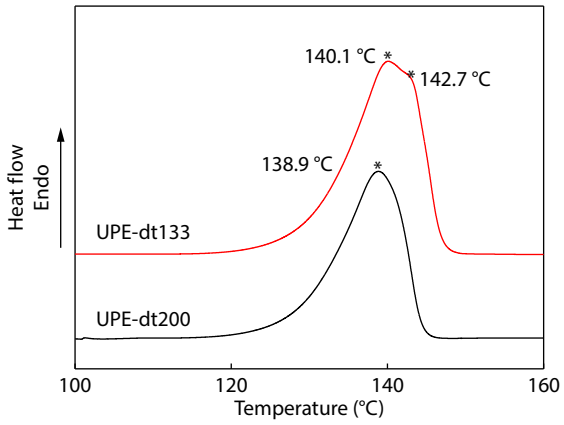

Fig. 3 DSC curves of UPE-dt200 and UPE-dt133.

Mechanical Response during Hot Stretching at Different Temperatures

The above SEM, DSC and Viscosity results all confirmed the successful reservation of shish crystals in UHMWPE films prepared by gel molding. Our subsequent investigation focuses on the mechanisms of structural evolution of UPE-dt200 and UPE-dt133 stretched at different temperatures. Fig. 4 shows the stress-strain curves of UPE-dt200 and UPE-dt133 stretched at different temperatures. UHMWPE films all show the typical three stages of elastic deformation, yield, and strain hardening when stretched at different temperatures. UPE-dt133 shows higher stress values than UPE-dt200 at different stretching temperatures. This suggests that the reserved shish crystals could significantly increase the breaking strength and Young's modulus of UHMWPE films. Additionally, it was found that UPE-dt133 has a faster increase of the stress during the hot stretching, which makes it enter the strain hardening stage earlier (200%–300%). This result indicates that the reserved shish crystals promote the transmission of stress between crystals, particularly during the strain hardening stage. As a result, UPE-dt133 has a more significant increase of stress before and after the strain hardening stage compared to UPE-dt200. It is notable that for both UPE-dt200 and UPE-dt133, when stretched at higher temperatures (120 and 130 °C), the stress is lower than those at 100 and 110 °C, this result is due to the increased mobility of molecular chains at higher temperatures.

SAXS Results

To further investigate the effect of reserved shish crystals on the

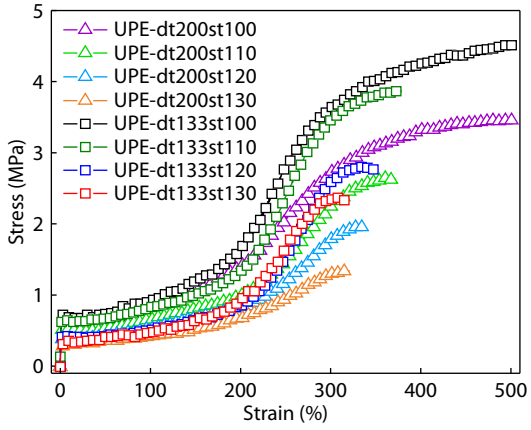

Fig. 4 Stress-strain curves of UPE-dt200 and UPE-dt133 hot stretched at different temperatures.

https://doi.org/10.1007/s10118-024-3143-3

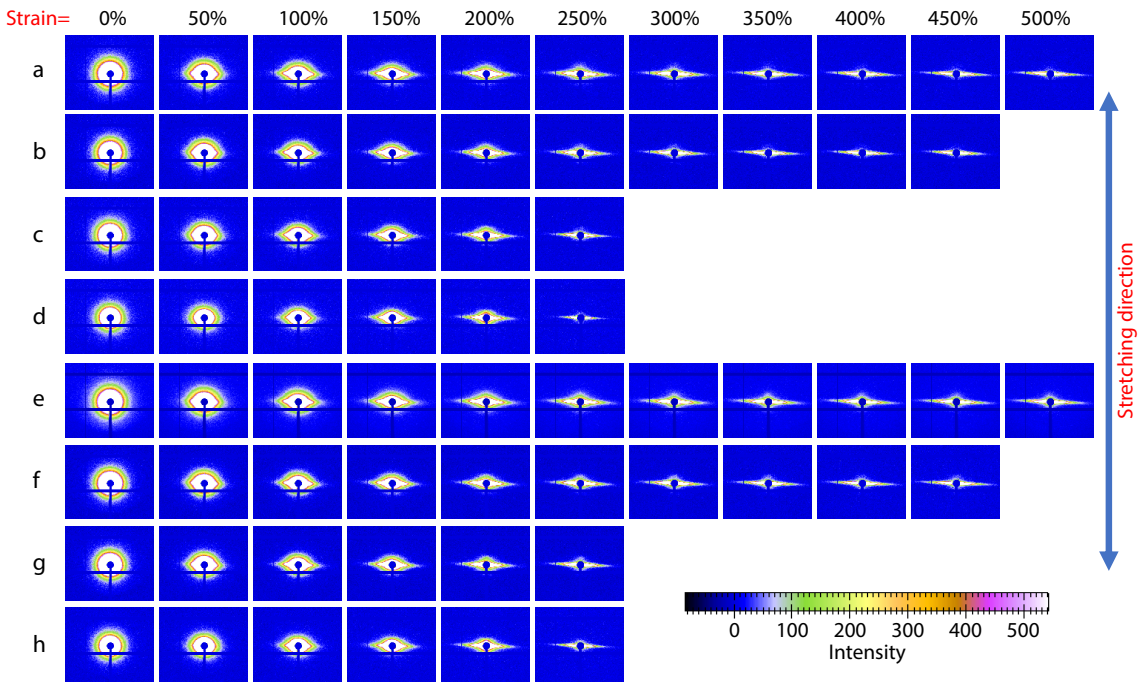

Fig. 5 *In-situ* 2D SAXS patterns of UPEdt200 and UPEdt133 stretched at different temperatures: (a) UPE-dt200st100, (b) UPE-dt200st110, (c) UPE-dt200st120, (d) UPE-dt200st130, (e) UPE-dt133st100, (f) UPE-dt133st110, (g) UPE-dt133st120, (h) UPE-dt133st130.

structural evolution and the properties during the hot stretching of UHMWPE low-entangled films. Fig. 5 shows the *in situ* 2D SAXS patterns of UPE-dt200 and UPE-dt133 stretched at different temperatures. As the stretching proceeds, both UPE-dt133 and UPE-dt200 evolve from initial scattering rings to ellipses and then to shuttle shapes along the equatorial direction. This indicates that the randomly oriented lamellae in the films gradually align along the stretching direction. Notably, no distinct kebab long-period signals were observed in the 2D SAXS patterns. This lack of long-period signals could be due to the presence of residual porosity in the low-entangled films caused by the extraction and drying process after gel molding, and consequently, during the hot stretching process, stretching-induced filling of these pores occurs with the fragmentation and recrystallization of lamellae, indicating that the shish-kebab crystals formed in the process of hot stretching of gel films are not as periodic as the shish-kebab crystals formed by traditional stretching of gel fibers.[63] Additionally, the 2D SAXS patterns reveal that UPE-dt133 shows stronger scattering signals along the stretching direction during hot stretching at different temperatures compared to UPE-dt200. This suggests that the reserved shish crystals in UPE-dt133 can accelerate the formation and evolution of shish-kebab crystals during the hot stretching.

Fig. 6 shows the scattering intensity ratio of crystals along the stretching direction (q_1) to those along the vertical direction (q_2) for UPE-dt200 and UPE-dt133 stretched at different temperatures. The initial Iq_1/Iq_2 for UPE-dt200 and UPE-dt133 show no significant increase, suggesting that the reserved shish crystals have not yet aligned along the stretching direction. As the stretching proceeds, UPE-dt133 shows faster increase in Iq_1/Iq_2 compared to UPE-dt200, this suggests that the reserved shish crystals in UPE-dt133 accelerate the crystal alignment along the stretching direction. When stretched at

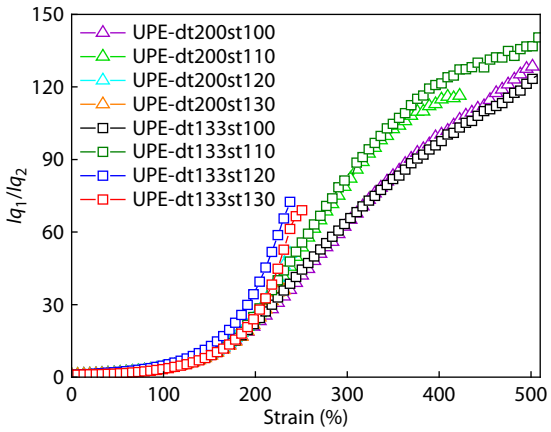

Fig. 6 Ratio of scattering intensity of crystals in the stretching direction (q_1) to crystals in the vertical stretching direction (q_2) for UPE-dt200 and UPE-dt133 stretched at different temperatures.

higher temperatures (12 and 130 °C), there is a more rapid increase of Iq_1/Iq_2, this result also confirmed the increased mobility of the molecular chains when stretched at 120 and 130 °C, which allows more chains to participate in the crystal growth and evolution. A similar trend in the scattering intensity is observed for UHMWPE high-entangled films with reserved shish crystals prepared by the compression molding.[40] A comparison of the two molding methods also indicates that reserved shish crystals are more effective in inducing the structural evolution of shish-kebab crystals in low-entangled systems.

USAXS Results

To understand more clearly the changes of the growth and evolution of shish-kebab crystals, we observe the growth and evo-

lution of shish-kebab crystals on a larger scale by *in situ* USAXS. Fig. 7 shows the *in situ* 2D USAXS patterns for UPE-dt200 and UPE-dt133 stretched at different temperatures. As the stretching proceeds, both UPE-dt200 and UPE-dt133 show shuttle shapes along the stretching direction. And UPE-dt133 shows more distinct patterns during the later stages of stretching. The shuttle shape observed in UPE-dt200 patterns is attributed to the gradual evolution of shish crystals formed along the stretching direction, while the shuttle shape observed in UPE-dt133 is attributed to the alignment of reserved shish crystals and newly formed shish crystals along the stretching direction.

Fig. 8 shows the average lengths (L_{shish}) and distributions (B_{Φ}) of shish crystals along the stretching direction for UPE-dt200 and UPE-dt133 stretched at different temperatures. UPE-dt200 shows a gradual decrease in L_{shish} and B_{Φ}. This is due to that the molecular chains are easily disentangled from the amorphous region and involved in the evolution from lamellae to shish-kebab crystals during the initial stage of hot stretching, during the later stage of hot stretching, only new, shorter shish crystals can be formed from the remaining molecular chains which are difficult to disentangle,[22] and the decrease of B_{Φ} is caused by the continuous alignment of shish crystals along the stretching direction during the hot stretching. In contrast, UPE-dt133 shows an initial increase followed by a decrease in L_{shish} during the hot stretching, the initial increase of L_{shish} suggests that the alignment of reserved shish crystals along the stretching direction during the hot stretching, as stretching proceeds, newly formed shish crystals are formed with a shorter L_{shish} than the reserved shish crystals, resulting in a decrease in L_{shish}.[38] During the hot stretching, both reserved and newly formed shish crystals gradually align along the stretching direction, resulting in a decrease in B_{Φ}. Comparing the results for L_{shish} and B_{Φ} between UPE-dt133 and UPE-dt200 at different stretching temperatures, it is observed that the transition point of L_{shish} in UPE-dt133 is earlier than that in UPE-dt200. This provides further evidence that UPE-dt133 starts the transition of shish-kebab crystals at a lower strain, which confirms the role of reserved shish crystals in promoting crystal transition. Additionally, the L_{shish} can be calculated for UPE-dt133 when stretched at 120 and 130 °C with a strain of 50%, but a higher strain of close to 100% is required when stretched at 100 and 110 °C. This also confirms that the increased mobility of the molecular chains when stretched at 120 and 130 °C allows easier alignment of the reserved shish crystals along the stretching direction during the hot stretching. And these reserved shish crystals, which align faster along the stretching direction, can also better induce the surrounding newly formed crystals to align along the stretching direction, which accelerates the transition of newly formed crystals into shish-kebab crystals. In contrast, high-entangled films with reserved shish crystals prepared by compression molding do not show a significant decrease in the later stage of stretching,[39] indicating that the high-entangled molecular chains do not disentangle during the hot stretching to promote the formation of new shish crystals. As a result, the structural evolution of low-entangled films prepared by gel molding with reserved shish crystals shows a faster structural evolution.

WAXD Results

Fig. 9 shows the *in situ* 2D WAXD patterns for UPE-dt200 and UPE-dt133 stretched at different temperatures, with the stretching direction being the meridian direction. The (110) and (200) crystalline planes of the PE orthogonal crystal system can be found from the inside out. As the stretching proceeds, the diffraction signals along the meridional direction gradually weaken, while the diffraction rings along the equatorial direction increase gradually, forming diffraction arcs and finally transforming into diffraction points.

Fig. 10 shows the crystallinity, the lateral size and orientation changes of the (110) crystal plane of UPE-dt200 and UPE-dt133 stretched at different temperatures. Before hot stretch-

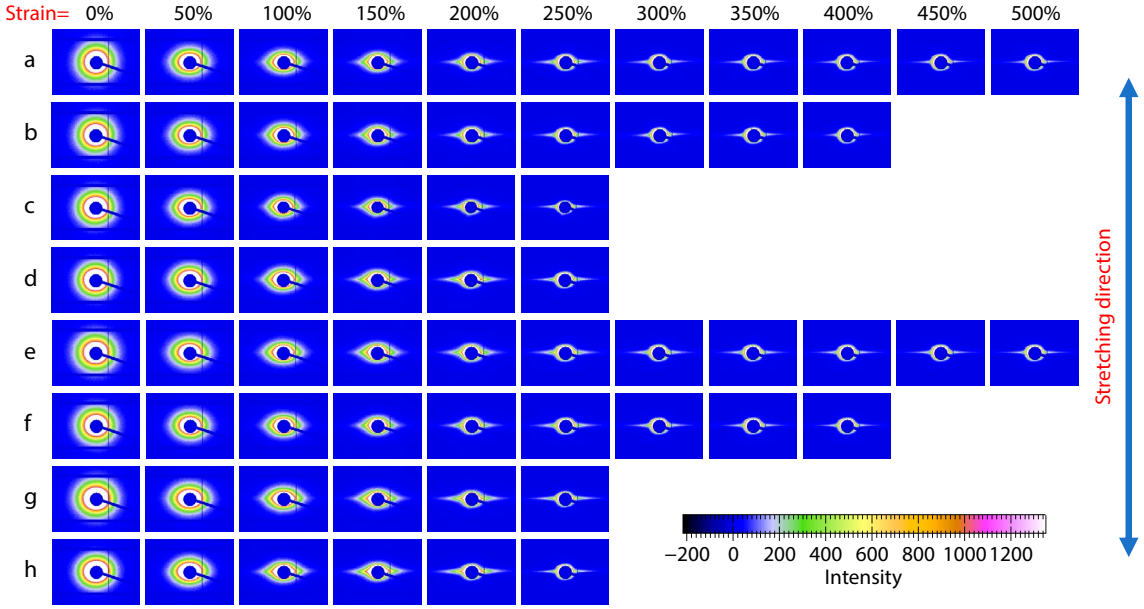

Fig. 7 *In-situ* 2D USAXS patterns of UPE-dt200 and UPE-dt133 stretched at different temperatures: (a) UPE-dt200st100, (b) UPE-dt200st110, (c) UPE-dt200st120, (d) UPE-dt200st130, (e) UPE-dt133st100, (f) UPE-dt133st110, (g) UPE-dt133st120, (h) UPE-dt133st130.

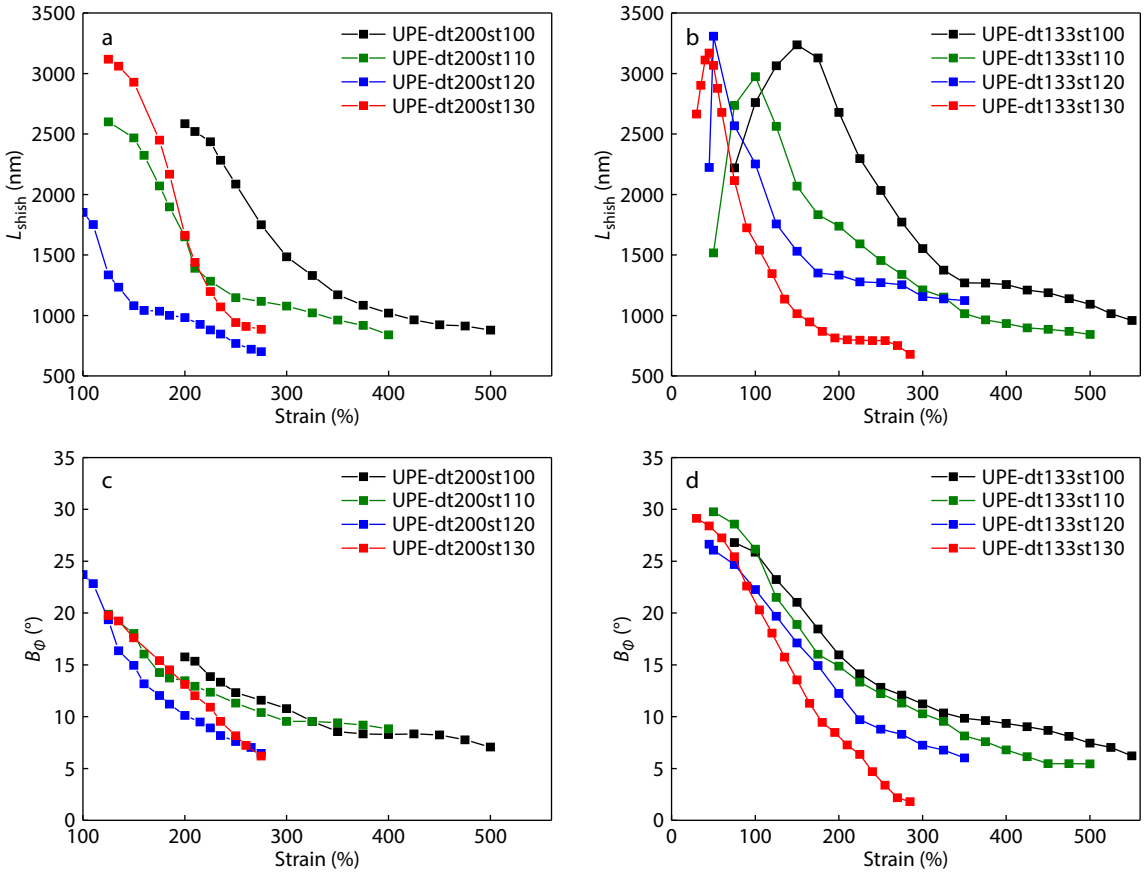

Fig. 8 Average shish length and distribution angle of UPE-dt200 and UPE-dt133 stretched at different temperatures.

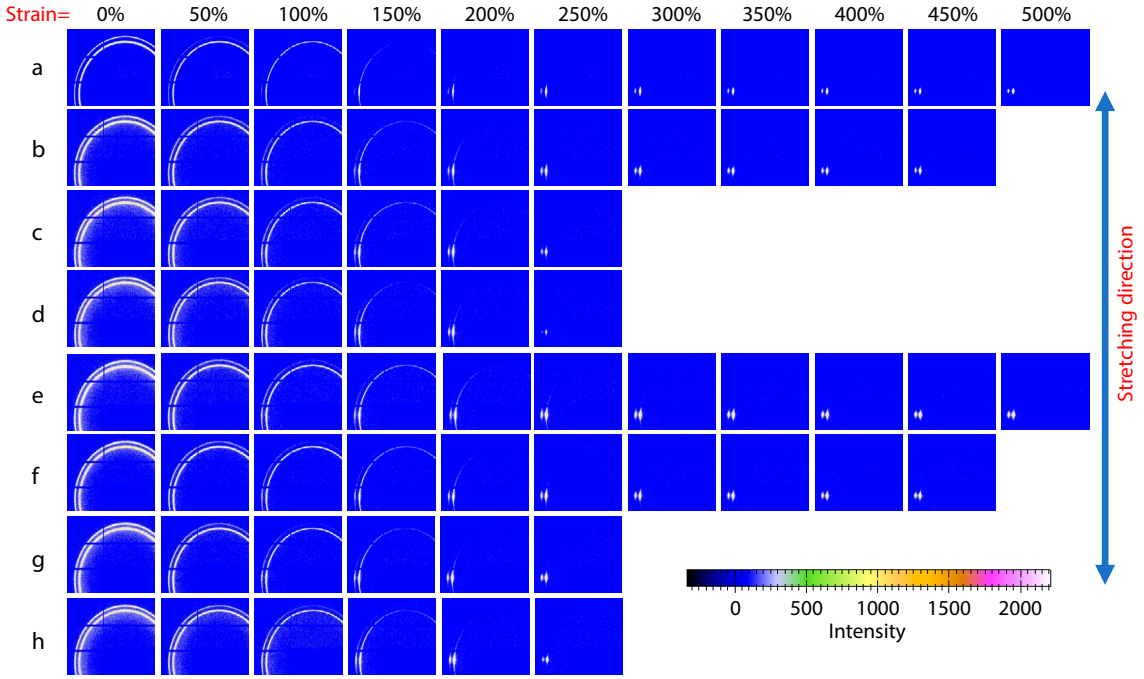

Fig. 9 *In situ* 2D WAXD patterns of UPE-dt200 and UPE-dt133 stretched at different temperatures: (a) UPE-dt200st100, (b) UPE-dt200st110, (c) UPE-dt200st120, (d) UPE-dt200st130, (e) UPE-dt133st100, (f) UPE-dt133st110, (g) UPE-dt133st120, (h) UPE-dt133st130.

https://doi.org/10.1007/s10118-024-3143-3

ing, the crystallinity of UPE-dt133 was consistently higher than that of UPE-dt200, indicating that the reserved shish crystals acted as nucleation points for crystal growth during the isothermal process. Additionally, before the hot stretching, higher crystallinity was observed at 100 and 110 °C, which were more conducive to crystal growth during the isothermal process.[64] The crystallinity of both UPE-dt200 and UPE-dt133 shows a decrease and then increase when stretched at 100 and 110 °C, with the decrease owing to the crystal fragmentation and the subsequent increase owing to the recrystallization. When the films were stretched at 120 and 130 °C, a rapid decrease was followed by a slow decrease, and then a rapid increase in crystallinity change. This result further confirms that the increased mobility of molecular chains when stretched at 120 and 130 °C leads to the melting and recrystallization of crystals during stretching, resulting in a faster decrease in crystallinity compared to crystal fragmentation when stretched at 100 and 110 °C,[40] and the slow decrease corresponds to the recrystallization to form some initial shish-kebab crystals that delay the decrease of crystallinity.[40] Figs. 10(a) and 10(b) show that the crystallinity increase of UPE-dt133 is faster than UPE-dt200 when stretched at dif-

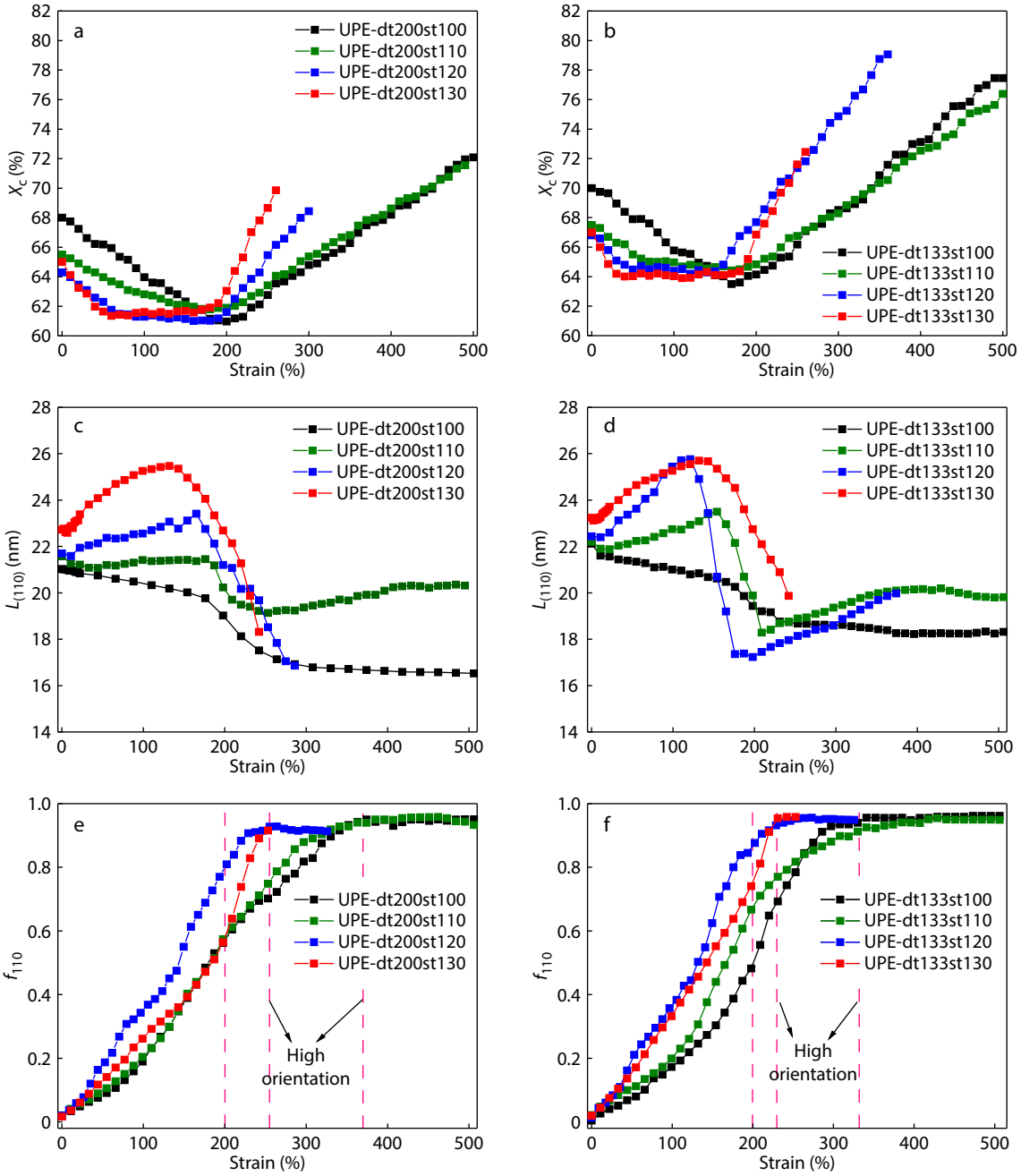

Fig. 10 (a, b) Crystallinity, (c, d) (110) crystalline plane lateral size and (e, f) orientation changes for UPE-dt200 and UPE-dt133 stretched at different temperatures.

https://doi.org/10.1007/s10118-024-3143-3

ferent temperatures. This also confirms that the reserved shish crystals can accelerate the formation and evolution of shish-kebab crystals, which is consistent with the mechanical results. Figs. 10(c) and 10(d) show the change of lateral size of UPE-dt200 and UPE-dt133 stretched at different temperatures. Before the hot stretching, UPE-dt133 and UPE-dt200 exhibit a larger initial lateral size when stretched at 120 and 130 °C, which is due to the higher temperatures favoring the growth of lamellae. In the early stages of the hot stretching, UPE-dt133 and UPE-dt200 show a gradual increase in lateral size when stretched at 120 and 130 °C, this result is owing to the recrystallization followed by crystal melting. Whereas a small decrease was observed when stretched at 100 °C, suggesting that the crystal changes are dominated by the crystal fragmentation when stretched at 100 °C, which is consistent with the continuous decrease in crystallinity at this temperature. As the stretching proceeds, UPE-dt133 and UPE-dt200 show a rapid decrease in lateral size when stretched at different temperatures, the decrease in the lateral size corresponds to the evolution from lamellae to shish-kebab structures, which is consistent with the rapid increase in crystallinity. Additionally, Figs. 10(c) and 10(d) show that the decrease in lateral size for UPE-dt133 at different stretching temperatures occurred earlier than for UPE-dt200. This also indicates that the reserved shish crystals accelerate the formation and evolution of shish-kebab structures, which is consistent with the change in crystallinity.

In the preceding SAXS results, we investigated that the faster increase of Iq_1/Iq_2 for UPE-dt133 than UPE-dt200 stretched at different temperatures was attributed to the accelerated transformation of crystals along the stretching direction because of reserved shish crystals. This finding is further supported by the WAXD results. Figs. 10(e) and 10(f) show the orientation changes of (110) crystal plane along the stretching direction for UPE-dt133 and UPE-dt200 stretched at different temperatures. During the initial stages of stretching, the orientation increased continuously, while in the later stages of stretching, it approached a plateau. Notably, the orientation reached values greater than 0.9, which indicates a highly oriented crystal structure. Before reaching a strain of 200%, the UPE-dt133 showed a faster orientation change than UPE-dt200 at all stretching temperatures except 100 °C. This indicates that the reserved shish crystals can induce crystal orientation along the stretching direction during the early stages of stretching, and the lower orientation observed for UPE-dt133 stretched at 100 °C is attributed to the lower temperature, which has a decreased mobility of molecular chains compared to 110–130 °C, resulting in a slower induction of crystal orientation by reserved shish crystals. While reaching a strain of 200%, UPE-dt133st100 exhibited a faster increase in orientation compared to UPE-dt200st100, which is due to the crystals growing around the reserved shish crystals gradually aligned along the stretching direction. Furthermore, UPE-dt133 reached a highly oriented crystal structure faster than UPE-dt200 stretched at different temperatures. And UPE-

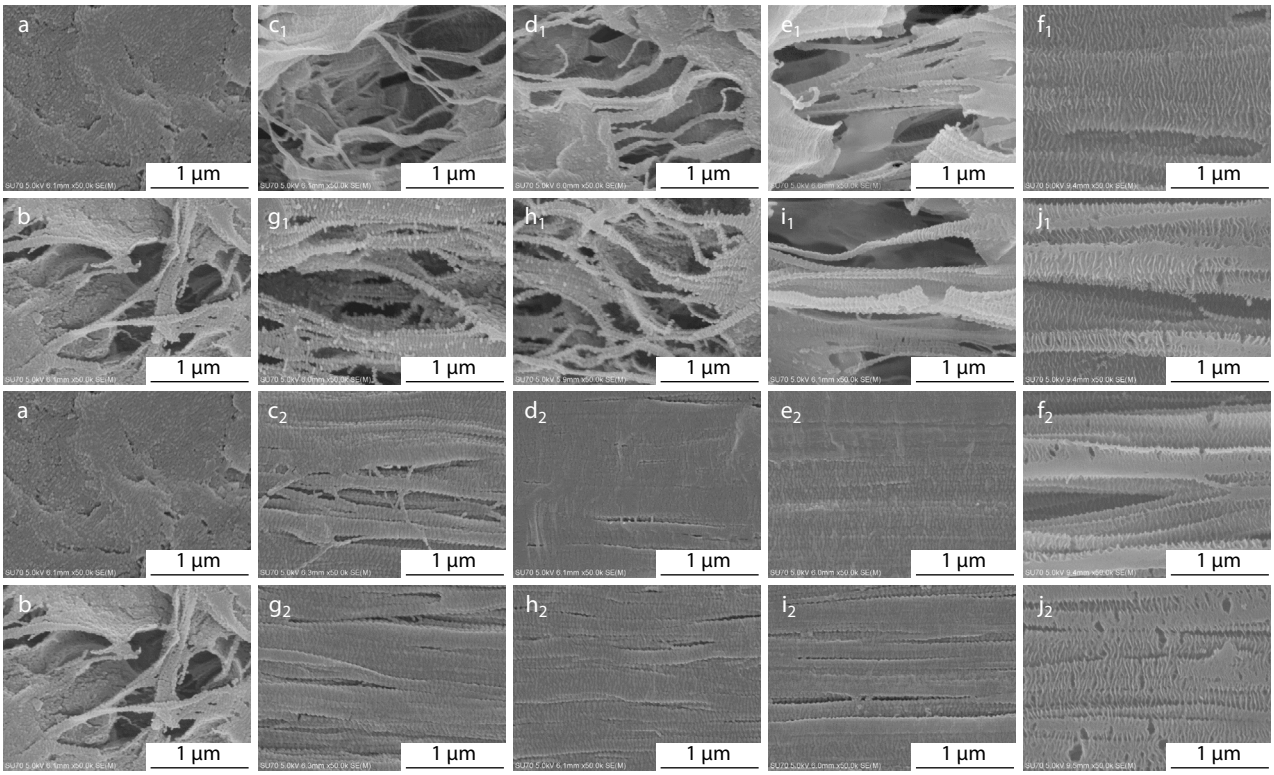

Fig. 11 SEM morphologies of UPE-dt200 and UPE-dt133 stretching to 100% and 300% at different temperatures. (a) UPE-dt200-0%, (b) UPE-dt133-0%, (c_1) UPE-dt200st100-100%, (d_1) UPE-dt200st110-100%, (e_1) UPE-dt200st120-100%, (f_1) UPE-dt200st130-100%, (g_1) UPE-dt133st100-100%, (h_1) UPE-dt133st110-100%, (i_1) UPE-dt133st120-100%, (j_1) UPE-dt133st130-100%, (c_2) UPE-dt200st100-300%, (d_2) UPE-dt200st110-300%, (e_2) UPE-dt200st120-300%, (f_2) UPE-dt200st130-300%, (g_2) UPE-dt133st100-300%, (h_2) UPE-dt133st110-300%, (i_2) UPE-dt133st120-300%, (j_2) UPE-dt133st130-300%. Horizontal direction is the stretching direction.

https://doi.org/10.1007/s10118-024-3143-3

dt133 can reached a highly oriented crystal structure faster when stretched at 120 and 130 °C because of the increased mobility of molecular chains. The WAXD results indicate that stretching at 120 and 130 °C resulted in faster evolution for shish-kebab structures compared to 100 and 110 °C, and the crystals aligned more easily along the stretching direction. This further confirms that the reserved shish crystals can induce the formation and evolution of shish-kebab crystals, particularly when stretched at 120 and 130 °C. In contrast, the UHMWPE high-entangled film with reserved shish crystals prepared by compression molding exhibit limited orientation. In some cases, they even show lower orientation than films without reserved shish crystals.[39] UHMWPE low-entangled films with reserved shish crystals prepared by gel molding exhibit more significant increases in orientation, and the crystals exhibit a highly oriented shish structures along the stretching direction, particularly in the later stages of the hot stretching. This further indicates that the UHMWPE low-entangled films show more inducement in promoting structural evolution during hot stretching.

Morphology Results

To provide a clearer description of the structural evolution in UHMWPE low-entangled films with reserved shish crystals stretched at different temperatures, Fig. 11 shows the SEM results of UPE-dt200 and UPE-dt133 before stretching, stretch to 100%, and 300%. Before hot stretching, the UPE-dt200-0% shows a morphology with disordered lamellae, while the UPE-dt133-0% shows a morphology with shish-kebab crystals. UPE-dt133-100% showed shish-kebab crystals and gradually aligned along the stretching direction when stretched at different temperatures. Conversely, UPE-dt200-100% mainly showed lamellae arrangements, which indicates that the reserved shish crystals induced the formation of shish-kebab crystals during the initial stages of stretching. UPE-dt133-300% shows highly oriented shish-kebab structures when stretched at different temperatures, some of these well-oriented shish-kebab structures are gradually transformed into shish crystals. In contrast, UPE-dt200-300% shows that the shish-kebab crystals along the stretching direction are not as uniform as those in UPE-dt133-300%. The SEM results show that stretching at 120 and 130 °C resulted in more orderly alignment of crystals along the stretching direction compared to stretching at 100 and 110 °C, which is consistent with the SAXS and WAXD results. The average long period and lamellae thickness of crystals measured from lots of SEM images and the results are shown in Table S1 in the electronic supplementary information (in ESI), which further indicates that the reserved shish crystals can promote the formation of well-organized shish-kebab crystals, and the shish-kebab crystals have a tendency to transform into shish crystals when stretched at 120 and 130 °C.

Melting Behavior Results

The above results indicate that the reserved shish crystals can accelerate the structural evolution of UHMWPE films. To further confirm the effect of reserved shish crystals on UHMWPE low-entangled films, Figs. 12(a) and 12(b) show the DSC curves for initial films and films stretched to different strains at 100, 110, 120 and 130 °C, respectively. The DSC curves of films with reserved shish crystals (dark curves) show a significant shift towards a higher temperature peak compared to those without shish crystals (light curves) at different temperatures from 100% to 300%. This indicates that the reserved shish crystals can accelerate the evolution from lamellae to shish-kebab crystals during the hot stretching. Additionally, the DSC results also show that the melting peaks are broader when stretched at 120 and 130 °C compared to 100 and 110 °C, which is also caused by the increased mobility of molecular chains when stretched at 120

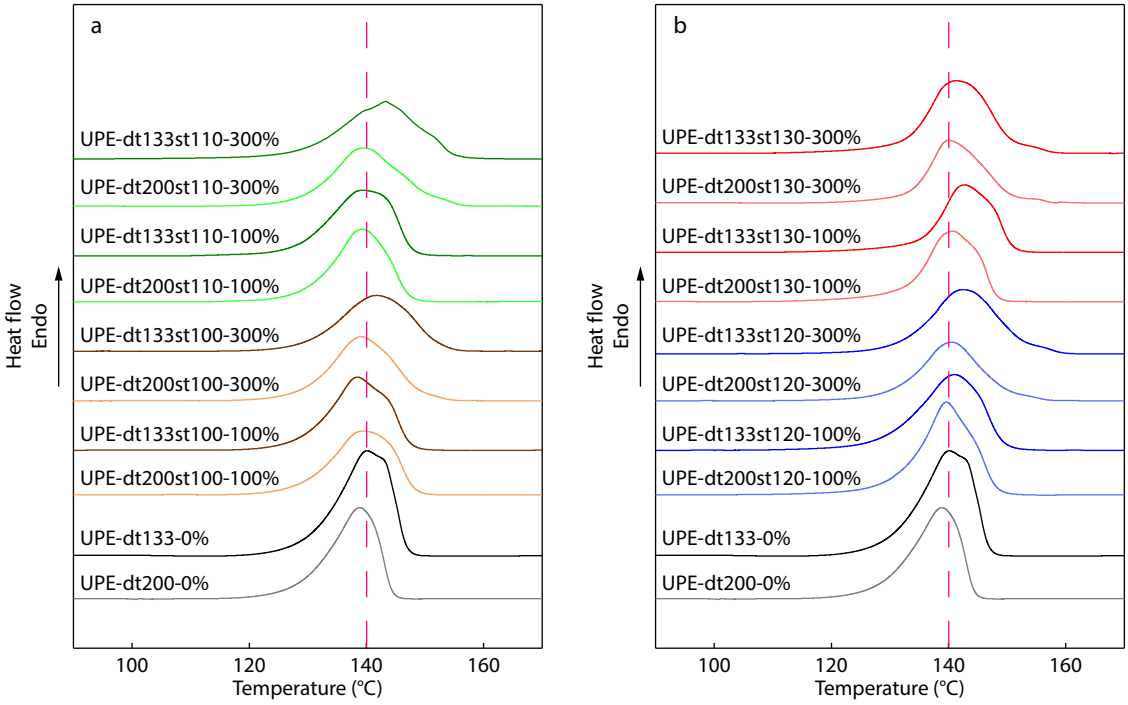

Fig. 12 DSC curves of UPE-dt200 and UPE-dt133 stretched to different strains at different temperatures and original UHMWPE films. (a) 100 and 110 °C; (b) 120 and 130 °C.

https://doi.org/10.1007/s10118-024-3143-3

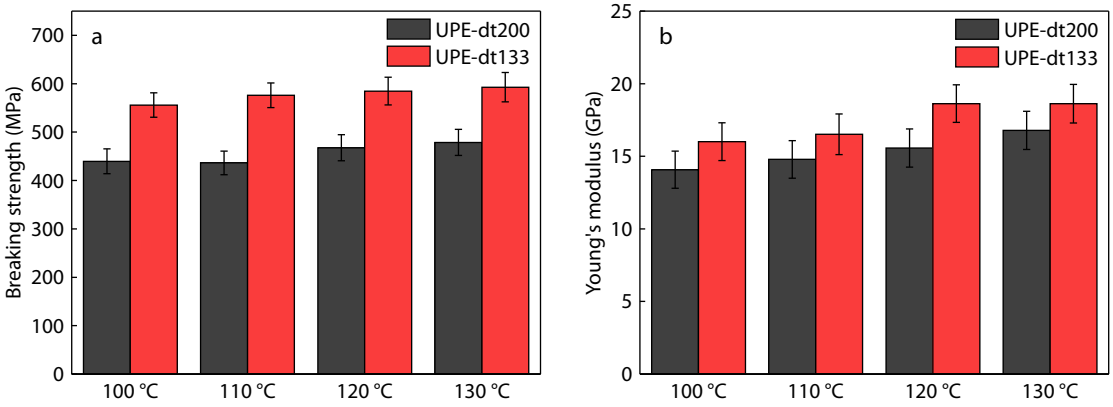

Fig. 13 (a) Breaking strength and (b) Young's modulus after stretching at different temperatures for UPE-dt200 and UPE-dt133.

and 130 °C, which allows more molecular chains to participate in the crystal growth and evolution, resulting in more shish-kebab crystals transform into highly-oriented shish crystals that show higher temperature peak. Compared to the UHMWPE film with reserved shish crystals prepared by compression molding,[39] UHMWPE low-entangled films with reserved shish crystals prepared by gel molding show a higher temperature peak at 142 or even 143 °C after stretching at different temperatures, indicating that the reserved shish crystals were more effective in inducing structural evolution for highly oriented shish crystals in the low-entangled system.

Breaking Strength and Young's Modulus

Figs. 13(a) and 13(b) show the breaking strength and Young's modulus of UPE-dt133 and UPE-dt200 after stretching at different temperatures. It can be seen that UPE-dt133 stretched at different temperatures shows higher breaking strength and Young's modulus compared to UPE-dt200. This indicates that the reserved shish crystals give a significant improvement in the mechanical properties of the films, which is consistent with the above conclusion that the reserved shish crystals can induce the structural evolution of UHMWPE gel films. Additionally, the breaking strength and Young's modulus show a higher value when stretched at 120 and 130 °C compared to 100 and 110 °C because of the shish-kebab crystals and the oriented lamellae show a greater alignment along the stretching direction due to the increased mobility of molecular chains, which result in a more organized crystal structure after the hot stretching. Compared to the UHMWPE high-entangled films with reserved shish crystals prepared by compression molding,[40] UHMWPE low-entangled films with reserved shish crystals prepared by gel molding show a 150% increase in breaking strength and a 600% increase in Young's modulus. This results fully indicates that the reserved shish crystals were more effective in promoting the formation and structural evolution of highly oriented shish crystals in the low-entangled system.

Mechanism of Structural Evolution of UHMWPE Low-entangled Films with Reserved Shish Crystals during Hot Stretching

The results of SAXS/USAXS/WAXD, SEM, DSC, breaking strength and Young's modulus stretched at different temperatures indicate that the reserved shish crystals can accelerate the formation and evolution of shish-kebab crystals, and the increased mobility of molecular chains can further promote the structural evolution of shish-kebab crystals. Fig. 14 shows the mechanism of structural evolution of UHMWPE low-entangled films with reserved shish crystals during hot stretching. Before crystallization, there are molecular chains and reserved shish crystals in UPE-dt133. During the crystallization, these reserved shish crystals act as nucleation to induce the growth of shish-kebab crystals, as a result, UPE-dt133 shows shish-kebab crystals and lamellae before stretching, while UPE-dt200 only shows disordered lamellae. In the middle stages of stretching, UPE-dt200 shows a gradual alignment of lamellae along the stretching direction when stretched at 100 and 110 °C, and the lamellae tend to align more easily along the stretching direction when stretched at 120 and 130 °C due to the increased mobility of molecular chains. As the stretching proceeds, UPE-dt200 shows evolution from lamellae to shish-kebab crystals with size reduced, and the disentangled molecular chains promote the formation of new short shish-kebab crystals, while stretching at 120 and 130 °C, in addition to the evolution from oriented lamellae to shish-kebab crystals, some highly oriented shish-kebab crystals gradually transform into highly oriented shish crystals. In contrast, in the middle stages of stretching, UPE-dt133 shows that the shish-kebab crystals growing from the reserved shish crystals gradually align along the stretching direction with lamellae oriented when stretched at 100 and 110 °C, while stretched at 120 and 130 °C, the shish-kebab crystals and the oriented lamellae show greater alignment along the stretching direction due to the increased mobility of molecular chains, resulting in small-sized shish-kebab crystals, and the oriented lamellae gradually transformed to shish-kebab crystals by the effect of the alignment of shish-kebab crystals formed by reserved shish crystals along the stretching direction. As the stretching proceeds, UPE-dt133 shows further orientation of shish-kebab crystals that growing from the reserved shish crystals, and further transforming into highly oriented shish crystals. Additionally, some oriented lamellae surrounding the reserved shish crystals gradually transformed into new shish-kebab crystals. While stretched at 120 and 130 °C, these shish-kebab crystals growing from reserved shish crystals and newly formed shish-kebab crystals complete their transformation from shish-kebab crystals to highly oriented shish crystals, and the highly oriented lamellae during the middle stretching not only transform into shish-kebab crystals, but also a portion of the regular shish-kebab crystals derived from lamellae undergo further transformation into shish crystals, the transformation of shish crystals derived from retained shish crystals and lamellae leads to highly oriented and well-

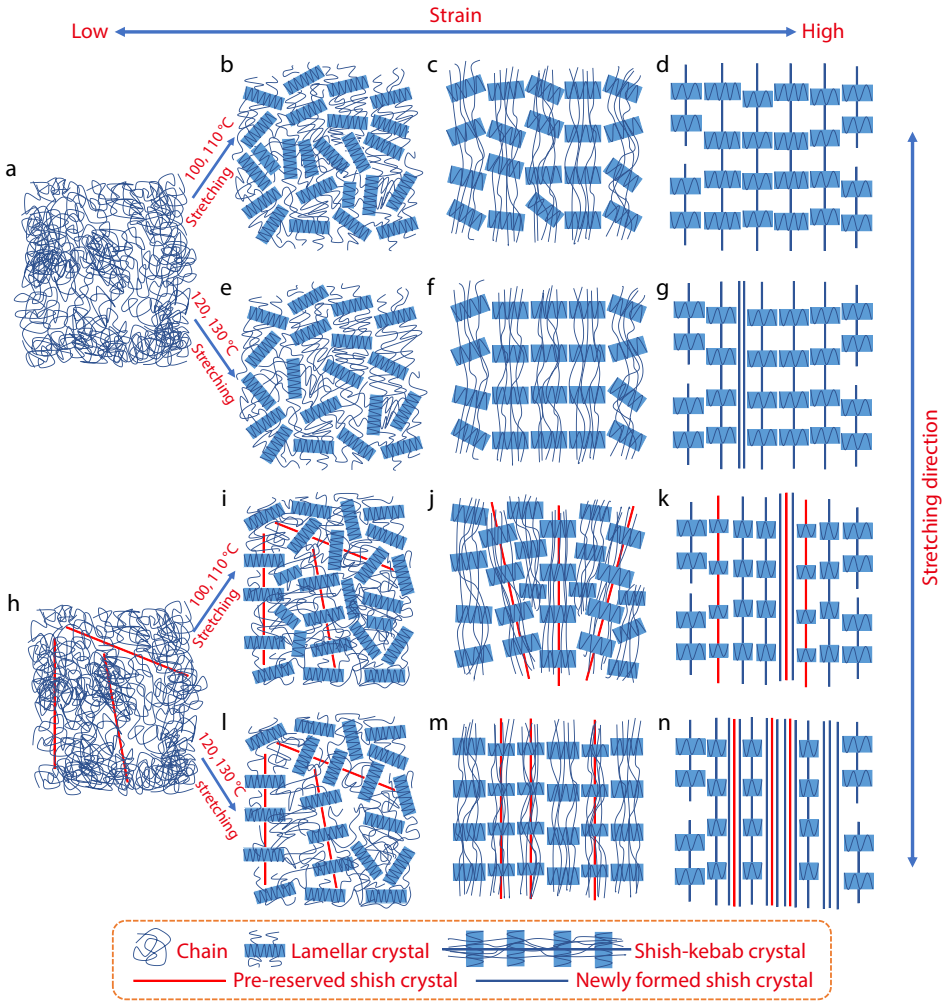

Fig. 14 Structural evolution mechanism of UHMWPE low-entangled films with and without reserved shish crystals stretched at different temperatures: (a) UPE-dt200-before crystallization, (b) UPE-dt200-100°C, 110 °C pre-stretching, (c) UPE-dt200-100°C, 110 °C mid-stretching, (d) UPE-dt200-100°C, 110 °C post-stretching, (e) UPE-dt200-120°C, 130 °C pre-stretching, (f) UPE-dt200-120°C, 130 °C mid-stretching, (g) UPE-dt200-120°C, 130 °C post-stretching, (h) UPE-dt133-before crystallization, (i) UPE-dt133-100°C, 110 °C pre-stretching, (j) UPE-dt133-100°C, 110 °C mid-stretching, (k) UPE-dt133-100°C, 110 °C post-stretching, (l) UPE-dt133-120°C, 130 °C pre-stretching, (m) UPE-dt133-120°C, 130 °C mid-stretching, (n) UPE-dt133-120°C, 130 °C post-stretching.

developed crystal structures in films after stretching at 120 and 130 °C. UHMWPE films with reserved shish crystals, prepared *via* gel molding, exhibit enhanced structural evolution and properties in comparison to those prepared via compression molding. The addition of paraffin oil and reserved shish crystals significantly reduces molecular chain entanglement during the processing of these films. Consequently, shish crystals align and orient more rapidly during hot stretching, resulting in a more improved shish-kebab structure as evidenced by WAXD and SEM results. Conversely, compression-molded films with reserved shish crystals show a lower content of induced shish crystals, with a gradual increase in L_{shish}. In contrast, the L_{shish} in gel-molded films initially increases and then decreases, suggesting the induction of numerous new shish-kebab crystals during hot stretching. This abundance of highly oriented shish-kebab crystals in gel-molded films contributes to improved thermal properties, breaking strength, and Young's modulus. Specifically, the melting point of gel-molded films after stretching is higher (142 °C to 143 °C) compared to compression-molded films (138 °C to 139 °C), with a 150% increase in breaking strength and a 600% increase in Young's modulus.[39,40]

CONCLUSIONS

In this study, UHMWPE low-entangled films with reserved shish crystals were prepared by gel molding, using the dissolution difference between shish crystals and lamellae. The structural evolution of UHMWPE low-entangled films with reserved shish crystals stretched at different temperatures were investigated by *in situ* SAXS/USAXS/WAXD measurements, as well as SEM, DSC, breaking strength and Young's modulus properties measurements. The results show that the reserved shish crystals can induce the formation and structural evolution of shish-kebab crystals for UHMWPE low-entangled films during the hot stretching, resulting in faster structural evolution, and higher thermal and mechanical properties compared to the UHMWPE low-entangled films without reserved shish crystals. Additionally, the reserved shish crystals are more effective in inducing the formation and structural evolution of shish-kebab crystals when

https://doi.org/10.1007/s10118-024-3143-3

stretched at 120 and 130 °C. This is due to the increased mobility of molecular chains, resulting in a more oriented and organized crystal structure after 120 and 130 °C stretching. Compared to UHMWPE high-entangled films with reserved shish crystals prepared by compression molding, the reserved shish crystals are more effective in promoting the formation and structural evolution of shish-kebab crystals in the low-entangled system. Consequently, the final thermal and mechanical properties of UHMWPE low-entangled films with reserved shish crystals prepared by gel molding are significantly improved. This study not only further investigates the structural evolution mechanisms of UHMWPE but also provides a new theoretical and experimental basis for UHMWPE products prepared by gel extrusion molding.

Conflict of Interests

The authors declare no interest conflict.

Electronic Supplementary Information

Electronic supplementary information (ESI) is available free of charge in the online version of this article at http://doi.org/10.1007/s10118-024-3143-3.

Data Availability Statement

The data that support the findings of this study are available from the corresponding author upon reasonable request. The author's contact information: wangzongbao@nbu.edu.cn.

ACKNOWLEDGMENTS

This work was financially supported by the National Natural Science Foundation of China (Nos. 52173021 and 52373038), Key Research and Development Programme of Zhejiang Province (No. 2023C01209) and S&T Innovation 2025 Major Special Programme of Ningbo (No. 2023Z079). The authors would like to appreciate the Shanghai Synchrotron Radiation Facility (SSRF) for the beamtime of SAXS, USAXS and WAXD.

REFERENCES

1 Wang, Z.; Ma, Z.; Li, L. Flow-induced crystallization of polymers: molecular and thermodynamic considerations. *Macromolecules* **2016**, *49*, 1505–1517.
2 Pennings, A. J.; Lageveen, R.; de Vries, R. S. Hydrodynamically induced crystallization of polymers from solution. *Colloid Polym. Sci*. **1977**, *255*, 532–542.
3 Hu, W. G.; Schmidt-Rohr, K. Characterization of ultradrawn polyethylene fibers by NMR: crystallinity, domain sizes and a highly mobile second amorphous phase. *Polymer* **2000**, *41*, 2979–2987.
4 Zhao, Y.; Zhu, Y.; Sui, G.; Chen, F.; Fu, Q. Tailoring the crystalline morphology and mechanical property of olefin block copolymer *via* blending with a small amount of UHMWPE. *Polymer* **2017**, *109*, 137–145.
5 Huang, Y. F.; Zhang, Z. C.; Xu, J. Z.; Xu, L.; Zhong, G. J.; He, B. X.; Li, Z. M. Simultaneously improving wear resistance and mechanical performance of ultrahigh molecular weight polyethylene via cross-linking and structural manipulation. *Polymer* **2016**, *90*, 222–231.
6 Dyer, S. R.; Lassila, L. V.; Jokinen, M.; Vallittu, P. K. Effect of fiber position and orientation on fracture load of fiber-reinforced composite. *Dent. Mater.* **2004**, *20*, 947–55.
7 Jordan, N. D.; Olley, R. H.; Bassett, D. C.; Hine, P. J.; Ward, I. M. The development of morphology during hot compaction of Tensylon high-modulus polyethylene tapes and woven cloths. *Polymer* **2002**, *43*, 3397–3404.
8 Marissen, R. Design with ultra strong polyethylene fibers. *Mater. Sci. Appl.* **2011**, *02*, 319–330.
9 Porter, R. S.; Kanamoto, T.; Zachariades, A. E. Property opportunities with polyolefins: a review. Preparations and applications of high stiffness and strength by uniaxial draw. *Polymer* **1994**, *35*, 4979–4984.
10 Shen, L.; Peng, M.; Qiao, F.; Zhang, J. L. Preparation of microporous ultra high molecular weight polyethylene (UHMWPE) by thermally induced phase separation of a UHMWPE/liquid paraffin mixture. *Chinese J. Polym. Sci.* **2008**, *26*, 653–657.
11 Xia, L.; Xi, P.; Cheng, B. A comparative study of UHMWPE fibers prepared by flash-spinning and gel-spinning. *Mater. Lett.* **2015**, *147*, 79–81.
12 Hu, S.; Feng, Y.; Yin, X.; Zou, X.; Qu, J. Structure and properties of UHMWPE products strengthened and toughened by pulse vibration molding at low temperature. *Polymer* **2021**, *229*, 124026.
13 Xiao, M.; Yu, J.; Zhu, J.; Chen, L.; Zhu, J.; Hu, Z. Effect of UHMWPE concentration on the extracting, drawing, and crystallizing properties of gel fibers. *J. Mater. Sci.* **2011**, *46*, 5690–5697.
14 Keum, J. K.; Zuo, F.; Hsiao, B. S. Formation and stability of shear-induced shish-kebab structure in highly entangled melts of UHMWPE/HDPE blends. *Macromolecules* **2008**, *41*, 4766–4776.
15 Xu, L.; Chen, C.; Zhong, G. J.; Lei, J.; Xu, J. Z.; Hsiao, B. S.; Li, Z. M. Tuning the superstructure of ultrahigh-molecular-weight polyethylene/low-molecular-weight polyethylene blend for artificial joint application. *ACS Appl. Mater. Interfaces* **2012**, *4*, 1521–1529.
16 Zhang, L.; Lu, C.; Dong, P.; Wang, K.; Zhang, Q. Realizing mechanically reinforced all-polyethylene material by dispersing UHMWPE *via* high-speed shear extrusion. *Polymer* **2019**, *180*, 121711.
17 Kakiage, M.; Fukagawa, D. Preparation of ultrahigh-molecular-weight polyethylene fibers by combination of melt-spinning and melt-drawing. *Mater. Today Commun.* **2020**, *23*, 100864.
18 Pennings, A. J.; Smook, J. Mechanical properties of ultra-high molecular weight polyethylene fibres in relation to structural changes and chain scissioning upon spinning and hot-drawing. *J. Mater. Sci.* **1984**, *19*, 3443–3450.
19 Yeh, J. T.; Lin, S. C.; Tu, C. W.; Hsie, K. H.; Chang, F. C. Investigation of the drawing mechanism of UHMWPE fibers. *J. Mater. Sci.* **2008**, *43*, 4892–4900.
20 Xu, H.; An, M.; Lv, Y.; Zhang, L.; Wang, Z. Structural development of gel-spinning UHMWPE fibers through industrial hot-drawing process analyzed by small/wide-angle X-ray scattering. *Polym. Bull.* **2017**, *74*, 1–16.
21 An, M.; Xu, H.; Lv, Y.; Gu, Q.; Tian, F.; Wang, Z. An in situ small-angle X-ray scattering study of the structural effects of temperature and draw ratio of the hot-drawing process on ultra-high molecular weight polyethylene fibers. *RSC Adv.* **2016**, *6*, 50373–51484.
22 Wang, Z.; An, M.; Xu, H.; Lv, Y.; Tian, F.; Gu, Q. Structural evolution

from shish-kebab to fibrillar crystals during hot-stretching process of gel spinning ultra-high molecular weight polyethylene fibers obtained from low concentration solution. *Polymer* **2017**, *120*, 244–254.
23 An, M.; Lv, Y.; Yao, G.; Zhang, L.; Wang, Z. Structural transformation from shish-kebab crystals to micro-fibrils through hot stretching process of gel-spun ultra-high molecular weight polyethylene fibers with high concentration solution. *J. Polym. Sci., Part B: Polym. Phys.* **2018**, *56*, 225–238.
24 Blais, P.; Manley, R. S. J. Morphology of Nascent Ziegler-Natta polymers. *Science* **1966**, *153*, 539–541.
25 Blais, P.; Manley, R. S. J. Morphology of nascent polyolefins prepared by Ziegler-Natta catalysis. *J. Polym. Sci., Part A: Polym. Chem.* **1968**, *6*, 291–334.
26 Manley, T. G. S. J. Morphology of nascent polyethylene prepared with the catalyst $VOCl_3(C_2H_5)_2AlCl$. *Polymer* **1972**, *66*, 627–635.
27 Chen, Y.; Liang, P.; Yue, Z.; Li, W.; Yang, Y. Entanglement formation mechanism in the POSS modified heterogeneous Ziegler-Natta catalysts. *Macromolecules* **2019**, *52*, 7593–7602.
28 Chen, Y.; Li, W.; Zhang, L.; Ye, C.; Tao, G.; Ren, C.; Jiang, B.; Wang, J.; Yang, Y. *In situ* synthesized self-reinforced HDPE/UHMWPE composites with high content of less entangled UHMWPE and high gradient-distributed oriented structures. *ACS Appl. Polym. Mater.* **2023**, *5*, 88–98.
29 Dermeneva, M.; Ivan'kova, E.; Marikhin, V.; Myasnikova, L.; Yagovkina, M.; Radovanova, E. In *X-ray analysis of compacted and sintered UHMWPE reactor powders*, Journal of Physics: Conference Series, **2018**; p 012058.
30 Chanzy, H. D.; Bonjour, E.; Marchessault, R. H. Nascent structures during the polymerization of ethylene. *Colloid Polym. Sci.* **1974**, *252*, 8–14.
31 Reneker, D. H.; Kataphinan, W.; Theron, A.; Zussman, E.; Yarin, A. L. Nanofiber garlands of polycaprolactone by electrospinning. *Polymer* **2002**, *43*, 6785–6794.
32 Bawn, C. E. H.; Ledwith, A.; McFarlane, N. Anionic polymerization of ethylene oxide in dimethyl sulphoxide. *Polymer* **1969**, *10*, 653–659.
33 Ingram, P.; Schindler, A. Morphology of as-polymerized polythylene II. Electron microscopy. *Macromol. Chem. Phys.* **1968**, *111*, 267–270.
34 Uehara, H.; Tamura, T.; Kakiage, M.; Yamanobe, T. Nanowrinkled and nanoporous polyethylene membranes *via* entanglement arrangement control. *Adv. Funct. Mater.* **2012**, *22*, 2048–2057.
35 Salari, M.; Pircheraghi, G. Interdiffusion versus crystallization at semicrystalline interfaces of sintered porous materials. *Polymer* **2018**, *156*, 54–65.
36 Jauffrès, D.; Lame, O.; Vigier, G.; Doré, F. Microstructural origin of physical and mechanical properties of ultra high molecular weight polyethylene processed by high velocity compaction. *Polymer* **2007**, *48*, 6374–6383.
37 An, M. F.; Xu, H. J.; Lv, Y.; Zhang, L.; Gu, Q.; Tian, F.; Wang, Z. B. The influence of chitin nanocrystals on structural evolution of ultra-high molecular weight polyethylene/chitin nanocrystal fibers in hot-drawing process. *Chinese J. Polym. Sci.* **2016**, *34*, 1373–1385.
38 An, M.; Xu, H.; Lv, Y.; Tian, F.; Gu, Q.; Wang, Z. The effect of chitin nanocrystal on the structural transition of shish-kebab to fibrillar crystals of ultra-high molecular weight polyethylene/chitin nanocrystal fibers during hot-stretching process. *Eur. Polym. J.* **2017**, *96*, 463–473.
39 Deng, B.; Wang, Z.; Chen, L.; Li, X. Influence of prereserved shish crystals on the structural evolution of ultrahigh-molecular weight polyethylene films during the hot stretching process. *Macromolecules* **2022**, *55*, 4600–4613.
40 Deng, B.; Chen, L.; Zhong, Y.; Li, X.; Wang, Z. The effect of temperature on the structural evolution of ultra-high molecular weight polyethylene films with pre-reserved shish crystals during the stretching process. *Polymer* **2023**, *267*, 125690.
41 Bartczak, Z.; Beris, P. F. M.; Wasilewski, K.; Galeski, A.; Lemstra, P. J. Deformation of the ultra-high molecular weight polyethylene melt in the plane-strain compression. *J. Appl. Polym. Sci.* **2012**, *125*, 4155–4168.
42 Diop, M. F.; Burghardt, W. R.; Torkelson, J. M. Well-mixed blends of HDPE and ultrahigh molecular weight polyethylene with major improvements in impact strength achieved *via* solid-state shear pulverization. *Polymer* **2014**, *55*, 4948–4958.
43 Huang, Y. F.; Xu, J. Z.; Li, J. S.; He, B. X.; Xu, L.; Li, Z. M. Mechanical properties and biocompatibility of melt processed, self-reinforced ultrahigh molecular weight polyethylene. *Biomaterials* **2014**, *35*, 6687–97.
44 Huang, Y. F.; Xu, J. Z.; Zhang, Z. C.; Xu, L.; Li, L. B.; Li, J. F.; Li, Z. M. Melt processing and structural manipulation of highly linear disentangled ultrahigh molecular weight polyethylene. *Chem. Eng. J.* **2017**, *315*, 132–141.
45 Deplancke, T.; Lame, O.; Rousset, F.; Aguili, I.; Seguela, R.; Vigier, G. Diffusion versus cocrystallization of very long polymer chains at interfaces: experimental study of sintering of UHMWPE nascent powder. *Macromolecules* **2013**, *47*, 197–207.
46 da Silva Chagas, N. P.; Lopes da Silva Fraga, G.; Marques, M. d. F. V. Fibers of ultra-high molecular weight polyethylene obtained by gel spinning with polyalphaolefin oil. *Macromol. Res.* **2020**, *28*, 1082–1090.
47 Tao, G. Exploring the entangled state and molecular weight of UHMWPE on the microstructure and mechanical properties of HDPE/UHMWPE blends. *J. Appl. Polym. Sci.* **2021**, *138*, 50741.
48 Gao, P.; Mackley, M. R. Effect of presolvent loading on the ultimate drawability of ultra-high molecular weight polyethylene. *Polymer* **1991**, *32*, 3136–3139.
49 Tian, Y.; Zhu, C.; Gong, J.; Yang, S.; Ma, J.; Xu, J. Lamellae break induced formation of shish-kebab during hot stretching of ultra-high molecular weight polyethylene precursor fibers investigated by in situ small angle X-ray scattering. *Polymer* **2014**, *55*, 4299–4306.
50 Hoogsteen, W.; Tenbrinke, G.; Pennings, A. J. DSC experiments on gel-spun polyethylene fibers. *Colloid Polym. Sci.* **1988**, *266*, 1003–1013.
51 Hammersley, A. P.; Svensson, S. O.; Thompson, A. Calibration and correction of spatial distortions in 2D detector systems. *Rev. Sci. Instr.* **1995**, *346*, 312–321.
52 Wunderlich, B.; Czornyj, G. A study of equilibrium melting of polyethylene. *Macromolecules* **1977**, *10*, 906–913.
53 Dai, H.; Yin, G. Z.; Zhao, F. J.; Bian, Z. X.; Xu, Y. J.; Zhang, W. B.; Miao, X. R.; Li, H. Facile synthesis and hierarchical assembly of polystyrene-block-poly (perfluorooctylethyl acrylates). *Polymer* **2017**, *113*, 46–52.
54 Fancher, C. M.; Hoffmann, C. M.; Frontzek, M. D.; Bunn, J. R.; Payzant, E. A. Probing orientation information using 3-dimensional reciprocal space volume analysis. *Rev. Sci. Instr.* **2019**, *90*, 013902.
55 Phillips, A. W.; Bhatia, A.; Zhu, P. W.; Edward, G. Shish formation and relaxation in sheared isotactic polypropylene containing nucleating particles. *Macromolecules* **2011**, *44*, 3517–3528.
56 Zhou, D.; Yang, S. G.; Lei, J.; Hsiao, B. S.; Li, Z. M. Role of stably entangled chain network density in shish-kebab formation in polyethylene under an intense flow field. *Macromolecules* **2015**, *48*, 6652–6661.
57 Perret, R.; Ruland, W. Single and multiple X-ray small-angle scattering of carbon fibres. *J. Appli. Crystallography* **1969**, *2*, 209–218.

https://doi.org/10.1007/s10118-024-3143-3

58 Ruland, W. Small-angle scattering studies on carbonized cellulose fibers. *J. Polym. Sci., Part C: Polym. Symp.* **1969**, *28*, 143–151.
59 Tang, Y.; Jiang, Z.; Men, Y.; An, L.; Enderle, H. F.; Lilge, D.; Roth, S. V.; Gehrke, R.; Rieger, J. Uniaxial deformation of overstretched polyethylene: *in-situ* synchrotron small angle X-ray scattering study. *Polymer* **2007**, *48*, 5125–5132.
60 Li, X.; Lin, Y.; Ji, Y.; Meng, L.; Zhang, Q.; Zhang, R.; Zhang, W.; Li, L. Strain and temperature dependence of deformation mechanism of lamellar stacks in HDPE and its guidance on microporous membrane preparation. *Polymer* **2016**, *105*, 264–275.
61 Shen, L.; Severn, J.; Bastiaansen, C. W. M. Drawing behavior and mechanical properties of ultra-high molecular weight polyethylene blends with a linear polyethylene wax. *Polymer* **2018**, *153*, 354–361.
62 Chiu, H. T.; Wang, J. H. Characterization of UHMWPE sol-gel transition by parallel plate rheometer and pulsed NMR. *Polymer* **1999**, *40*, 6859–6864.
63 Lv, F.; Chen, X.; Wan, C.; Su, F.; Ji, Y.; Lin, Y.; Li, X.; Li, L. Deformation of ultrahigh molecular weight polyethylene precursor fiber: crystal slip with or without melting. *Macromolecules* **2017**, *50*, 6385–6395.
64 Lv, R.; He, Y.; Xie, K.; Hu, W. Crystallization rates of moderate and ultrahigh molecular weight polyethylene characterized by flash DSC measurement. *Polym. Int.* **2020**, *69*, 18–23.

https://doi.org/10.1007/s10118-024-3143-3